Title

Centrifuge Modeling of Soil-Structure Interaction in Energy Foundations

Journal

Journal of Geotechnical and Geoenvironmental Engineering, 140(4)

ISSN

1090-0241

Authors

Stewart, Melissa A
McCartney, John S

Publication Date

2014-04-01

DOI

10.1061/(asce)gt.1943-5606.0001061

Peer reviewed

CENTRIFUGE MODELING OF SOIL-STRUCTURE INTERACTION IN ENERGY FOUNDATIONS

By Melissa A. Stewart, M.S., S.M.ASCE[1] and John S. McCartney, Ph.D., P.E., M.ASCE[2]

Abstract: This study presents a centrifuge modeling approach to characterize the transient thermo-mechanical response of energy foundations during heating-cooling cycles in order to provide data for calibration and validation of soil-structure interaction models. This study focuses on the response of a scale-model energy foundation installed in an unsaturated silt layer with end-bearing boundary conditions. The foundation response was assessed using embedded strain gages and thermocouples. Other variables monitored include foundation head displacements, soil surface displacements, and changes in temperature and volumetric water content in the unsaturated silt at different depths and radial locations. Measurements during the initial heating process indicate that the thermal axial stress is greater near the toe of the foundation due to the restraint associated with mobilization of side shear resistance along the length of the foundation. The thermal axial strains were close to the free-expansion thermal strain near the soil surface and decreased with depth. The thermal axial displacements calculated by integrating the thermal axial strains correspond well with the independently-measured head displacements. The mobilized side stresses calculated from the thermal axial stresses increased with height and were consistent with the shear strength of unsaturated silt. During successive heating-cooling cycles, slight decreases in upward thermal head displacement were observed due to changes in stiffness of the unsaturated soil due to thermally-induced water flow away from the foundation and potential down-drag effects. However, little change in the thermal axial stress was observed during the heating-cooling cycles.

[1] Graduate Research Assistant, Department of Civil, Environmental and Architectural Engineering, University of Colorado Boulder, UCB 428, Boulder, CO 80309
[2] Associate Professor and Lyall Faculty Fellow, Department of Civil, Environmental and Architectural Engineering, University of Colorado Boulder, UCB 428, Boulder, CO 80309

INTRODUCTION

Energy foundations, or drilled-shaft foundations that incorporate heat exchange elements, provide necessary structural support for buildings and act as heat sources or sinks for building heating and cooling systems using the same construction materials (Brandl 1998; Ennigkeit and Katzenbach 2001; Laloui et al. 2003; Brandl 2006). Energy foundations are a practical strategy to reduce the installation cost of ground-source heat exchange systems, which has been identified as one of the major barriers to implementation of this energy efficiency technology (Hughes 2008). However, an issue that should be carefully characterized is the potential for foundation movements due to thermal expansion and contraction of the foundation element or surrounding soil. Further, soil-structure interaction may restrain foundation movements, leading to generation of thermally induced stresses. The mechanisms of thermo-mechanical soil-structure interaction have been documented in several full-scale case histories in the field (Laloui et al. 2006; Bourne-Webb et al. 2009; Laloui 2011; Bouazza et al. 2011; Amatya et al. 2012; McCartney and Murphy 2012). In addition, thermo-mechanical soil-structure interaction analyses (Knellwolf et al. 2011) and thermo-elastic finite element analyses (Laloui et al 2006; Regueiro et al. 2012) have been developed that permit prediction of changes in axial displacement, strain, and stress in energy foundations during heating and cooling. The different analyses require empirical data for calibration of parameters and verification of predictions, which can often be difficult to obtain from full-scale case histories due to uncertain soil stratigraphy effects, varying foundation geometries, uncertain installation effects, and complex end-restraint boundary conditions.

The experience obtained from full-scale energy foundation studies can be complemented with the characterization of scale-model energy foundations in a geotechnical centrifuge to measure empirical parameters for soil-structure interaction analyses in carefully controlled

46 conditions, or to develop a database of information for validation of analyses. In centrifuge
47 modeling tests, the properties of scale-model foundations and soil layers can be carefully
48 controlled and different configurations can be considered for lower costs that full-scale testing in
49 the field. Centrifuge modeling also permits incorporation of dense instrumentation arrays to
50 capture thermo-mechanical effects in the energy foundation as well as thermo-hydro-mechanical
51 effects in the surrounding soil, both of which are necessary to validate predictions from finite
52 element analyses. Centrifuge modeling may be especially relevant when considering the
53 behavior of energy foundations in some soil deposits that may have nonlinear behavior, such as
54 soft clays or unsaturated soils. An advantage of centrifuge modeling over full-scale foundation
55 testing is that scale-model energy foundations can be loaded to failure to destructively
56 characterize the effects of temperature on the load-settlement curve and the back-calculated
57 ultimate side shear resistance and end bearing (McCartney and Rosenberg 2011). McCartney and
58 Rosenberg (2011) observed an increase in the ultimate capacity of energy foundations with
59 increasing temperature, which was proposed to be due to an increase in side shear resistance
60 resulting from differential lateral expansion of the energy foundation into the surrounding soil.
61 The objective of this study is to present a centrifuge modeling approach to quantify the
62 thermo-mechanical soil-structure interaction behavior of a centrifuge-scale energy foundation
63 installed in an unsaturated silt layer during cyclic heating and cooling. The energy foundation
64 considered in this study has an end-bearing boundary condition, in which the tip of the
65 foundation is resting on a rigid layer, and contains embedded strain gages and thermocouples to
66 measure distributions in strain and temperature. The head of the foundation is permitted to
67 expand freely under a constant applied load. These conditions represent a typical energy
68 foundation installed beneath a light structure. Results from this test, as well as others following

69 the same approach, can be used to understand the role of energy foundation end-restraint
70 boundary conditions on the magnitude and distribution of thermally induced axial strains,
71 displacements, and stresses. Further, the results can be used to delineate the advantages and
72 limitations of using centrifuge physical modeling to study thermo-mechanical soil-structure
73 interaction problems in energy foundations.

74 ## BACKGROUND

75 ### Soil-Structure Interaction in Energy Foundations

76 As an energy foundation is heated or cooled, it may expand or contract, respectively,
77 depending on the restraint boundary conditions. For unconstrained conditions, the thermal axial
78 strain can be calculated as follows:

$$\varepsilon_{T,unconstrained} = \alpha_c \Delta T \quad (1)$$

79 where α_c is the coefficient of linear thermal expansion of reinforced concrete, and ΔT is the
80 change in temperature. Thermal strain is defined as positive for compression to be consistent
81 with geotechnical conventions. Accordingly, α_c for reinforced concrete will be negative as
82 structural elements expand during heating (positive ΔT). The coefficient of linear thermal
83 expansion of unreinforced concrete ranges from 9 to -14.5 με/°C depending on the aggregate
84 mineralogy, while that of the steel reinforcements is approximately -11.9 to -13 με/°C (Bourne-
85 Webb et al. 2009; Stewart 2012). Because these values are relatively similar, significant
86 differential thermal strains are not expected in reinforced concrete. The value of $\varepsilon_{T,unconstrained}$ is
87 an upper limit on the thermal axial strains that can occur in the reinforced concrete due to heating
88 or cooling. If the energy foundation were fully constrained by the end-restraint boundary
89 conditions or the mobilized side shear resistance, the thermal axial strain would be zero. In this

90 case, the change in temperature of the energy foundation would generate the maximum value of
91 thermal axial stress $\sigma_{T,constrained}$, which can be calculated as follows:

$$\sigma_{T,constrained} = -E\alpha_c \Delta T \quad (2)$$

92 where E is the Young's modulus of the reinforced concrete. The boundary conditions for energy
93 foundations are likely between unconstrained and constrained conditions, due to soil-structure
94 interaction and the finite stiffness restraint of an overlying structure. The thermal axial strains ε_T
95 in energy foundations will be between the free expansion and fully constrained limit states. In
96 this case, the thermal axial stresses σ_T induced during a change in temperature can be calculated
97 as follows:

$$\sigma_T = E\left(\varepsilon_T - \alpha_c \Delta T\right) \quad (3)$$

98 During heating, the thermal axial strains in the energy foundation will be negative (expansive)
99 and less than $\varepsilon_{T,unconstrained}$, so the thermal will be positive (compressive). For energy foundations
100 embedded in soil or rock, the side shear resistance, end bearing, and stiffness restraint of the
101 overlying building will lead to different distributions in thermal axial stresses and strains.
102 Several full-scale tests have used different approaches to evaluate the distributions in thermal
103 axial strain and stress in energy foundations. Laloui et al. (2006), Laloui and Nuth (2006),
104 Bourne-Webb et al. (2009), Laloui (2011), and Amatya et al. (2012) evaluated the stresses and
105 strains in full-scale energy foundations loaded axial from the surface using a load frame for
106 different temperature changes. Bouazza et al. (2011) and Wang et al. (2012) used a combination
107 of Osterberg cells embedded in an energy foundation to translate a section of the shaft upward
108 and downward to characterize changes in side shear resistance with temperature. McCartney and
109 Murphy (2012) evaluated the stresses and strains in full-scale energy foundations installed
110 beneath a building during typical heat pump operations, which incorporates actual head end-

111 restraint boundary conditions. The current study follows the first approach, in which the energy
112 foundation is heated and cooled back to ambient temperature within a load frame.

113 Bourne-Webb et al. (2009) proposed hypothetical representations of the mechanisms of
114 thermo-mechanical soil-structure interaction in "floating" energy foundations that have no end
115 bearing, and Amatya et al. (2012) extended these representations to cases with non-zero end-
116 bearing (semi-floating and end-bearing conditions). In these hypotheses, a floating foundation is
117 expected to expand about it center during uniform heating, an end-bearing foundation is expected
118 to expand upward from the base, and a semi-floating foundation is expected to have an
119 intermediate response. Knellwolf et al. (2011) referred to the point of zero thermal axial
120 displacement in the foundation as the null point, and noted that this is an important parameter in
121 thermo-mechanical soil-structure interaction analyses. The hypothetical representations of soil-
122 structure interaction mechanisms are useful when evaluating field measurements and the results
123 from analyses, especially when differentiating the effects of temperature from those of
124 mechanical loading on the distributions in axial stress and side shear resistance. Although the
125 results from full-scale tests generally confirm the hypothetical representations, centrifuge
126 modeling permits isolation of the effects of complex end-restraint boundary conditions, different
127 side shear resistance mechanisms (frictional vs. cohesive), issues such as thermal dragdown of
128 surrounding soils.

129 **Centrifuge Modeling of Energy Foundations**

130 Centrifuge modeling relies on the concept of geometric similitude, which assumes that a full-
131 scale prototype soil layer will have the same stress state as a model-scale soil layer that is N
132 times smaller when spinning in a geotechnical centrifuge at a centripetal acceleration that is N
133 times larger than that of earth's gravity (Ko 1988; Taylor 1995). The centripetal acceleration

134 generates increased body forces in the scale-model. Geometric similitude can be employed to
135 extrapolate the load-settlement behavior and thermal soil-structure interaction phenomena of
136 scale-model energy foundations to those representative of full-scale prototype foundations in the
137 real world. After scaling the length of the foundation by a factor of 1:N (model:prototype),
138 strains in the foundation scale by a factor of 1:1, and forces scale by a factor of $1:N^2$ (Ko 1988;
139 Taylor 1995).

140 One issue in modeling energy foundations is that the temperature does not depend on the
141 increased body forces in the centrifuge. Spatial measurements of temperature in dry quartz sand
142 surrounding a cylindrical heat source during centrifugation at different g-levels by Krishnaiah
143 and Singh (2004) confirm that centrifugation does not lead to a change in the heat flow process.
144 However, if the dimensions associated with the spatial distribution of heat flow were scaled from
145 model to prototype scale (assuming the same thermal conductivity in both cases), the time
146 required for heat flow by conduction would be N^2 times faster in the centrifuge model ($1:N^2$).

147 Saviddou (1988) derived the scaling factor for the time required for heat flow for the case of
148 one-dimensional heat conduction in Cartesian coordinates using the diffusion equation, which
149 only involved scaling of the length. The same scaling factor of N^2 observed by Krishnaiah and
150 Singh (2004) was obtained. An implication of geometric similitude is that a greater volume of
151 soil surrounding the model-scale foundation will be affected by changes in temperature in a
152 given period of time than in a full-scale prototype. As soils change in volume with temperature, a
153 greater zone of soil around the foundation will be affected. Accordingly, the effects of
154 differential volume change of the foundation and soil may be emphasized in a centrifuge
155 modeling test. From this perspective, centrifuge modeling may provide a worst-case scenario for

156 temperature effects on soils surrounding an energy foundation, especially after reaching steady-
157 state conditions.

158 One solution to address the scaling conflict is to calibrate numerical finite element
159 simulations of the tests using the model-scale measurements. However, the experimental
160 approach can be modified depending on the goals of the test so that the prototype results can be
161 used for calibration of simple load-transfer analyses. If the goal of testing is to evaluate the
162 impact of temperature on the load-settlement curve of the foundations considering the role of the
163 surrounding soil, time should be provided to reach steady-state conditions. This is the only
164 approach that should be used for soft soils that experience plastic volume changes during
165 heating. This would provide a worst-case scenario as both the foundation and soil may
166 experience thermo-mechanical deformations that may affect soil-structure interaction. However,
167 as it may take a significant amount of time to reach steady-state conditions, this approach may
168 not be practical in centrifuge testing. An alternative that could be used when evaluating the
169 behavior of energy foundations in stiff soils or dry sands would be to wait until the foundation
170 reaches a steady temperature. In this case the load-settlement curve would only be representative
171 of transient conditions. Although this may not fully capture the effects of the soil on soil-
172 structure interaction, the behavior of energy foundation during transient heating and cooling is
173 still relevant as full-scale energy foundations often experience temperature reversals (McCartney
174 and Murphy 2012). Rosenberg (2010) measured the load-settlement curves of energy
175 foundations in compacted silt after the foundation reached a steady-state temperature, even
176 though the surrounding silt did not fully reach steady-state conditions, especially at a distance of
177 several foundation diameters away. When evaluating the impact of temperature on the thermal
178 axial strain distribution in energy foundation in stiff soils, tests can be performed until the

thermal axial strains within the foundation stabilize while its temperature is held constant. This was the intention of the approach followed in this study to evaluate changes in foundation behavior during transient changes in temperature over a short period of time.

MATERIALS

Scale-Model Energy Foundation

A scale-model energy foundation having a length of 533 mm and a diameter of 50.8 mm was constructed for this study. When the foundation is installed in the centrifuge container used in this study, which can accommodate a 533 mm-thick soil layer, its tip rests on the base of the container, so it is referred to as an end-bearing foundation. A centrifuge acceleration of 24 was used in this study, so the corresponding prototype-scale foundation length is 12.8 m with a diameter of 1.22 m. A schematic cross-sectional view of the foundation is shown in Figure 1.

Although drilled shafts are typically cast in place in soil, the model energy foundation was precast outside of the soil layer due to the large amount of instrumentation, cables, and heat exchanger tubing within the assembly. The pre-cast foundation can also be reused in subsequent tests, and can be tested outside of the soil layer to characterize its thermal and mechanical properties. The reinforcing cages for the model foundation was constructed from a hoop of steel wire mesh having a uniform opening size of 6.35 mm and a diameter of 40 mm. A cardboard tube having an inside diameter of 50.8 mm was used as a form for the foundation, permitting a concrete cover of 5 mm on the sides and 12.7 mm on the top and bottom. Cable stays (zip ties) were used to provide spacing between the reinforcing cage and the cardboard tube.

Three heat exchanger loops (3 inlets and 3 outlets) were installed in the foundation so that the distribution of heat across the circumference of the foundation would be as uniform as possible. Perfluoroalkoxy (PFA) heat exchanger tubes having an inside diameter of 3.175 mm were used

because they can accommodate high fluid pressures under high temperatures (830 kPa at 65°C) while remaining flexible. The inlet and outlet branches of each tubing loop were attached on the inside of the reinforcing cages, approximately opposite from each other. At the bottom of the foundation, the loops of tubing were pulled to the inside perimeter of the reinforcing cage to avoid segregation of concrete during placement and to ensure that the center of the foundation would be monolithic concrete.

Embedded strain gages and thermocouples were attached to the inside of the reinforcing cage of the model foundation at the locations shown in Figure 1, with two gages at each depth on opposite sides of the foundation. The strain gages used in this study were model CEA-13-250UW-350 obtained from Vishay Precision Group. These particular gages were selected because their coefficient of thermal expansion is similar to that of steel, and because they are designed to have a stable response during cyclic heating, considering gage resilience and error due to variations in temperature (Vishay Precision Group, personal communication 2011). The gages were first attached with temperature resistant M-Bond AE-15 adhesive to 30 mm-long steel tabs having a dog-bone shape with a hole punched at either end. This adhesive is cured at an elevated temperature of 85 °C, which makes it less likely to slip during cyclic heating than other adhesives that cure at room temperature. The gage was then covered with Teflon tape and the central part of the tab containing the gage was coated with M-Coat J, which is a flexible coating that protects against most fluids and mechanical damage during insulation. The steel tabs were then attached to the inside of the reinforcing cage. Near the top of the foundation, the strain gage leads were connected to a cable with shielded, twisted wire pairs to minimize the potential effects of electrical noise associated with the loading system. Miniature thermocouples (Omega fine wire Type K Model STC-TT-K-36 3C) were embedded within the foundation at the same

depths as the strain gages on one side of the foundation. The thermocouples were placed in contact with the steel tabs.

After centering of the reinforcing cage (with the heat exchanger tubing and instrumentation attached) within the cardboard mold, concrete having a mix ratio of 1:1.7:2.3:1 (water:cement:fine-aggregate:coarse-aggregate) was poured into the mold. No admixtures were included. The fine aggregate was conventional concrete sand, while the coarse aggregate was gravel having a maximum particle size less than 6 mm. The relatively large fraction of sand and the smaller size of the coarse aggregate is expected to lead to a softer response than the concrete used in full-scale drilled shafts, but this was necessary so that the concrete could flow around the instrumentation in the small-diameter foundation and through the openings in the reinforcing cage. After thorough mixing, the concrete was poured into the cardboard tube atop a shake table, and a rod was used to ensure even distribution of aggregates. The completed reinforced concrete foundation was placed in a curing room for 15 days, after which the cardboard tubing was removed. Most of the concrete strength gain was expected over this time in the curing room, although the foundation as not tested in the centrifuge until more than a month after construction.

A comprehensive set of characterization tests were performed on the pre-cast foundation to determine the mechanical and thermal properties of the reinforced concrete, the detailed results of which are presented in Stewart (2012). The first test involved application of incremental axial loads under room temperature conditions, taking care to properly level the foundation and center the load to avoid bending. The mechanical strains measured during application of an axial load of 700 kPa were variable, but gage-specific calibration factors were defined using the overall axial deformation of the foundation measured using a linearly-variable deformation transformer (LVDT). Tests were repeated to ensure that the variability was not due to seating conditions, and

248 care was taken to minimize the potential for bending. The Young's modulus determined using
249 the corrected strain data was 7.17 GPa. As expected, this value is lower than that of reinforced
250 concrete used in full-scale energy foundations (~30 GPa) because of the lower fraction of coarse
251 aggregate.

252 The energy foundation was then heated to a temperature of 62 °C by circulating fluid through
253 the heat exchange tubes within the foundation while maintaining a constant axial stress of
254 439 kPa. The foundation was permitted to expand freely under this axial stress, permitting
255 definition of the coefficient of linear thermal expansion of the foundation using the LVDT. The
256 value of α_c calculated from the LVDT measurements was found to be -7.5 με/°C, where με is
257 micro-strain (m/m × 10^6), with compressive strain defined as positive. Although the temperature
258 of each of the gages was within 2 °C during the heating test, the thermal response of each strain
259 gage was different, likely due to differences in curing of the adhesive bonding the strain gage to
260 the steel tab, or due to differential thermal expansion of the gage, adhesive, and the steel tab.
261 However, because the thermal axial strain should theoretically be the same at each location along
262 the length of the foundation for free expansion, thermal correction factors were defined using the
263 reading from the LVDT and the gage specific temperature. The thermal correction developed in
264 a subsequent study by Goode (2013) was used to reinterpret the strains reported by Stewart
265 (2012). Before application of the thermal correction factors, the gages were corrected for the
266 thermal offset error specific to this batch of gages and for differential expansion of the steel tabs
267 (α_s = -8.5 με/°C) and concrete which was assumed to be the same as the foundation overall
268 (α_c = -7.5 με/°C).
269

Soil

Soil obtained from the Bonny dam near the Colorado-Kansas border was used in the energy foundation test in this study. Relevant geotechnical properties of Bonny silt are summarized in Table 1, and additional information on the compaction curve, shear strength, soil-water retention curve, and shear modulus can be obtained from Stewart (2012). The liquid and plastic limits of the soil measured according to ASTM D 4318 are 26 and 24, and the fines content of this soil is 84%, so this soil classifies as ML (inorganic silt) according to the Unified Soil Classification System (USCS). The silt has a specific gravity G_s of 2.6. The reasons for using this soil in this study are that it has low plasticity, so temperature is not expected to lead to changes in soil-pore water interactions (i.e., diffuse double layer effects). Further, it has a high fines content so the silt will behave like a low-permeability material where thermal consolidation may occur.

Although a wider suite of soil preparation and saturation conditions are currently under investigation, the tests performed in this study involve a soil layer prepared using compaction to permit fast model preparation times and to reach uniform initial unit weight and water content distributions with height at the beginning of the tests. Further, compaction was expected to lead to a stiff soil response that would not lead to significant long-term settlement under the change in stress associated with centrifuge testing. The soil layer was prepared by compacting silt having a gravimetric water content of 14% in 76.2 mm-thick lifts around the foundation to reach a target dry density of 1451 kg/m^3. A vibratory hammer with a flat-plate adaptor having a width of 75 mm was used to compact the soil around the foundation to reach lifts with a final thickness of 75 mm. The centrifuge test was performed on the soil layer in as-compacted (unsaturated) conditions.

EXPERIMENTAL SETUP

Container and Load Control System

A schematic of the container used in this study to evaluate the thermo-mechanical strain distributions in the end-bearing energy foundation is shown in Figure 2. The container is a cylindrical aluminum tank with an inside diameter of 0.6 m, wall thickness of 13 mm, and a height of 0.54 m. A 13 mm-thick insulation sheet was wrapped around the container to prevent heat transfer through the sides of the cylinder (no-flow boundary). The bottom of the container permits some loss of heat, but it was preferred not to install insulation beneath the container to provide a stiff platform for loading. All sides of the container are impermeable, and post-test analysis of gravimetric water content values and measurements from embedded water content sensors indicated very little change in soil water content except near the foundation. The load frame consists of two steel frames mounted atop a rectangular steel platform. A horizontal brushed DC electric motor mounted between the steel frames is used to apply vertical loads to the top of the foundation through a coupling to a vertical worm drive. The applied load was measured using a load cell attached to the shaft of the worm drive, and a force-feedback control loop implemented using a National Instruments motor control module was used to maintain a constant axial load during testing. Additional pictures of the container and load frame are shown in Stewart (2012).

Soil Instrumentation

The locations of instrumentation incorporated into the centrifuge container are shown in Figure 2. An LVDT was placed on top of the foundation and three others were placed on the soil surface at different radial distances from the foundation. The LVDTs were mounted on cantilever arms connected to a support beam across the top of the container. The LVDTs, each having a

range of ±12.7 mm, were used to measure the self-weight settlement of the soil layer as well as a potential settlement basin created by movement of the foundation in the soil. The LVDT readings reported by Stewart (2012) were corrected to account for the change in the ambient temperature of the centrifuge chamber. Goode (2013) observed that the ambient temperature of the centrifuge led to a phantom model-scale settlement in mm of $0.0246\Delta T_{ambient}$, where $\Delta T_{ambient}$ is the change in temperature of the centrifuge chamber from the beginning of the test.

Four thermocouple profile probes equipped with six thermocouples at different locations along the probe were inserted into the soil at different radial locations from the foundation. The probes were passed through the support beam and were used to measure transient changes in temperature of the soil surrounding the foundation to assess heat transfer processes. Dielectric sensors (model EC-TM from Decagon Devices), capable of inferring the volumetric water content and temperature of the soil, were placed in the soil layer during compaction in a vertical array 50.8 mm away from the foundation at different depths, and in a horizontal array at a depth of 266.7 mm. These sensors were useful in monitoring thermally induced water flow in the unsaturated soil layer away from the foundation, and provided a backup measurement of soil temperatures.

Foundation Temperature Control System

The temperature control system used in this study was developed so that the energy foundation would reach a desired value. A heat pump, operated outside the centrifuge, was used to control the temperature of fluid circulating through the scale-model foundation. The F25-ME refrigerated/heated circulator manufactured by Julabo, Inc. was connected to the foundation via the hydraulic slip ring stack as shown in Figure 3. The heat pump consists of an automated temperature control system and circulating pump, with a working temperature range of -28 to

200 °C. The circulating pump can supply a pressure up to 38 kPa and a flow rate up to 16 l/min. An in-line high-capacity cartridge flow pump was attached to the inflow line to double the flow rate, which is important to ensure turbulent flow conditions in the heat exchange tubing and to overcome potential friction losses through the slip ring stack. Pure ethylene glycol was used as the heat exchange fluid because it could be safely circulated through the hydraulic slip rings of the centrifuge, which are intended for oil-based fluids only. The ethylene glycol has a thermal conductivity of 0.258 W/m°C and a viscosity ranging from 0.1 to 3.8 cP for temperatures from 30 to 71 °C. The foundation flow valve and bypass flow valve shown in Figure 3 are critical components used to control the temperature of the foundation. In order to pre-heat the ethylene glycol, the bypass valve was opened while the foundation flow valve was closed. This permitted the fluid in the supply and return lines to reach a steady-state temperature. The foundation and bypass flow valves were opened or closed in increments using LabView machine control software, which supplied varying flow rates of pre-heated fluid to the foundation. The temperatures of the fluid entering and exiting the foundation are monitored using pipe-plug thermocouples, as these temperatures permit evaluation of the heat energy input into the foundation. The average flow rate of the ethylene glycol during testing at elevated temperatures was 5 ml/s.

EXPERIMENTAL PROCEDURES

After assembly of the container within the load frame on the centrifuge basket, the centrifuge was spun to a target centripetal acceleration of 24 g's (defined at the center of the container). After the LVDTs on the foundation indicated that it was at equilibrium, a prototype-scale axial load of 443 kN (axial stress of 384 kPa) was applied to the end-bearing foundation to simulate a

360 constant building load. Because load-control conditions were employed, the top of the
361 foundation was free to deform upward or downward during cyclic heating.

362 After the foundation settlement due to application of the building load ceased, the foundation
363 was heated in increments. The inlet and outlet fluid temperatures (at the point the fluid enters and
364 exits the foundation) during this process are shown in Figures 4(a), along with the ambient air
365 temperature of the soil surface. The difference in inlet and outlet fluid temperatures reflects the
366 heat shed from the fluid into the foundation and surrounding soil, but these temperatures are
367 otherwise not important to consider as they fluctuated frequently to maintain a constant
368 foundation temperature. The ambient temperature was relatively steady during testing, showing a
369 temperature rise of less than 4 °C due to the friction of the centrifuge moving through the air in
370 the centrifuge chamber. The temperatures at different depths in the end-bearing foundation
371 measured using the embedded thermocouples are shown in Figure 4(b). Different from the fluid
372 temperatures, the foundation temperature is relatively stable as the temperature was stepped up in
373 increments to 39°C. The thermocouples at the top and bottom of the foundation show slightly
374 lower temperatures than those in the center of the foundation due to higher heat flow through the
375 steel base and because of the surface boundary conditions. Nonetheless, the temperature along
376 the length of the foundation is relatively uniform. After reaching a temperature of 39 °C, the
377 foundation was cooled back to ambient temperature, then reheated in four cycles.

378 **EXPERIMENTAL RESULTS**

379 Comparisons of the average foundation temperature and the temperatures in the middle of the
380 soil layer at different radial locations are show in Figure 4(c). The temperatures of the soil,
381 measured by the thermocouple profile probes in the case of the end-bearing foundation lag
382 behind the foundation temperatures due to the heat flow process. Further, they do not reach the

same magnitude of temperature as that of the foundation, even at a radial distance of 50.8 mm from the foundation. During the time that the foundation experienced changes in temperature of 19 °C, the soil experienced a maximum increase in temperature of approximately 5 °C. This small change in temperature may still have led to thermo-mechanical deformations of the silt. Uchaipichat and Khalili (2009) characterized the isotropic thermal volume change of compacted silt, and observed a transition in behavior from elastic expansion to plastic contraction during heating of compacted silt between net stresses of 100 and 150 kPa. Accordingly, for the stress-state in this study (average vertical net stress of approximately 120 kPa), the compacted silt may show either thermal expansion or contraction depending on the depth.

A time series of the axial stress applied to the head of the end-bearing foundation is shown in Figure 5(a), along with the average foundation temperature. Although a feedback loop was used to control the axial load, the system is particularly stiff, so minor vibrations occasionally led to instability. There were two occasions when the system became unstable and applied stresses greater than the target value. However, the head displacements and the thermal axial strains shown in Figures 5(b) and 5(c), respectively, indicate that the temporary increase in axial stress led to elastic mechanical deformations of the foundation and did not have a major impact on the thermal expansion of the foundation at the end of each heating phase. The prototype head displacement in Figure 5(b) was calculated by zeroing the model-scale head displacement at the end of spin-up and multiplying the scale factor of 24. The thermal head displacement was then calculated by zeroing the prototype head displacement at the start of the heating stages. As expected, the prototype head displacements indicate downward (positive) head movement during application of the mechanical load, and an upward head movement during heating. The foundation did not return to its original location during cooling as it was not cooled back to

406 ambient temperature. During successive heating cycles, a slight decrease in the amount of
407 upward head movement was observed.

408 The measurements from the LVDT on the soil surface at a model-scale distance of 76.2 mm
409 are also shown in Figure 5(c). Although not shown, the soil surface experienced an elastic
410 model-scale settlement of 0.48 mm during spin-up of the centrifuge. Over the course of the test,
411 an additional model-scale soil surface settlement of 0.19 mm occurred, corresponding to the
412 4.5 mm of prototype-scale soil surface settlement shown in Figure 5(c). This corresponds to a
413 vertical strain of 0.14%. The soil surface settlement does not appear to be correlated to the
414 temperature changes in the energy foundation. Nonetheless, the differential settlement between
415 the foundation and soil may have led to drag-down effects that may partially explain the slight
416 decrease in axial expansion during the heating stages.

417 The thermal axial strains were defined by zeroing the strain readings at the beginning of
418 heating and applying the thermal correction factors obtained from 1-g tests. The mechanical axial
419 strains for both foundations are reported by Stewart (2012), and are not included here because
420 their magnitude was insufficient to draw conclusions as to the distribution in side shear
421 resistance due to mechanical loading. The thermal axial strains indicate consistently negative
422 (expansive) strains in the foundation during heating which followed the same trends as the
423 imposed temperatures, even during heating cycles, as the foundation was never cooled below the
424 initial ambient temperature. The magnitude of the thermal axial strains were consistently lower
425 than the free expansion strain of the foundation $\varepsilon_{T,unconstrained}$ defined using Eq. (1).

426 The changes in volumetric water content at different depths in the soil layer at a model-scale
427 radial location of 50.8 mm are shown in Figure 5(d). The results in this figure indicate that
428 shortly after heating started, the soil adjacent to the foundation started to become wetter as water

429 is driven away from the foundation, with greater water flow near the top of the foundation. The
430 maximum increase in volumetric water content of 0.02 m^3/m^3 corresponds to an increase in
431 degree of saturation from 0.59 to 0.64. It is reasonable to assume that the soil closest to the
432 foundation decreased in volumetric water content by a similar amount, leading to a decrease in
433 degree of saturation from 0.59 to 0.54. The drying process of the soil closest to the foundation
434 will lead to an increase in effective stress, leading to an increase in ultimate side shear resistance.

435 ## ANALYSIS OF RESULTS

436 The thermal axial strains were synthesized to define profiles with height for different changes
437 in temperature during the initial heating stages, as shown in Figure 6(a). In general, the largest
438 thermal axial strains are observed near the top of the foundation, as the foundation is able to
439 expand freely as the axial stress was applied in load-control conditions. The thermal axial strains
440 at the top of the foundation (depth of zero) in this figure were calculated using the value of α_c for
441 the reinforced concrete, while the rest of the thermal axial strain values were obtained from the
442 measurements in Figure 5(c). The smallest thermal axial strain in the end-bearing foundation was
443 observed near the bottom of the foundation, which reflects greater constraint of foundation
444 movement. This is possibly due to the higher lateral stresses in the soil at the base of the
445 foundation.

446 Assuming that the thermal axial displacement was zero at the base of the container, which is
447 reasonable due to the relatively rigid base, the thermal axial strains were integrated over the
448 length of the foundation to define the thermal axial displacement at different depths, as follows:

$$\delta_{T,i} = \delta_{T,i-1} + \frac{1}{2}\left(\varepsilon_{T,i-1} + \varepsilon_{T,i}\right)\Delta l \qquad (4)$$

449 where $\delta_{T,i}$ is the thermal axial displacement at the midpoint between two gages at different
450 depths, $\varepsilon_{T,i}$ is the thermal axial strain at gauge i, and Δl is the distance between two gages. The

thermal axial displacement profiles calculated using Eq. (4) are shown in Figure 6(b), along with the thermal head displacements from Figure 5(b) at a depth of zero. The thermal axial displacement profiles obtained from the strain gages correspond reasonably well with the measured thermal head movement, indicating a nonlinear increase in thermal axial displacement with height. As mentioned, the location of the smallest thermal axial displacement is referred to as the null-point (Knellwolf et al. 2011), which represents the point about which the foundation expands during heating. The location of the smallest thermal axial displacement in the end-bearing foundation is located at the bottom of the foundation, as expected from the hypothetical representations of soil-structure interaction proposed by Amatya et al. (2012).

Thermal axial stress profiles for the end-bearing foundation calculated using Eq. (3) are shown in Figure 6(c). The greatest thermal axial stresses in the end-bearing foundation occur near the base of the foundation, slightly above the location of the null-point. The nonlinear change in stress with depth is due to the mobilized side shear stresses at the silt-foundation interface, which may also be affected by the increased radial stresses during heating (McCartney and Rosenberg 2011). The compacted silt is relatively stiff, and has a uniform density along the length of the foundation. Some drainage may have occurred during centrifugation and heating, making the soil near the toe have a greater undrained shear strength. In a natural soil deposit, it would be expected that drained conditions would occur, leading to a distribution in side shear resistance following the shape of the effective stress distribution in the soil layer. Nonetheless, the thermal stress distributions in the scale-model foundation corresponds well with those observed in field tests on end-bearing foundations by Laloui et al. (2006), Bourne-Webb et al. (2009), and McCartney and Murphy (2012). These observations confirm the utility of centrifuge

473 modeling in defining soil-structure interaction data during transient temperature changes that can
474 be used to calibrate and validate numerical analyses.

475 The mobilized side shear stresses at different depths can be calculated without the use of a
476 load-transfer analysis because the head of the energy foundation was permitted to freely expand
477 during heating. This would not have been the case if the energy foundation were restrained by
478 the stiffness of an overlying structure, as the thermal axial stress at the foundation head would
479 not be zero (Knellwolf et al. 2011). For the case of zero thermal axial stress at the head of the
480 foundation, the mobilized side shear stress $f_{s,mob}$ can be calculated as follows:

$$f_{s,mob,j} = \frac{\left(\sigma_{T,j-1} - \sigma_{T,j}\right) D}{4\Delta l} \tag{5}$$

481 where j is a counter from the top of the foundation, D is diameter of the foundation, and Δl is the
482 distance between two locations of known thermal axial stress. The distribution in mobilized side
483 shear stress with height calculated from the thermal axial stresses in Figure 6(c) is shown in
484 Figure 7(a). The maximum mobilized side shear stress is less than the shear strength expected for
485 unsaturated silt (Uchaipichat and Khalili 2009), and the mobilized side shear stress increases
486 with height consistent with the strain distribution within the energy foundation during heating.
487 The total mobilized side shear forces calculated by integrating the profiles of mobilized side
488 shear stress in Figure 7(a) are shown in Figure 7(b) as a function of the change in temperature.
489 The total mobilized side shear force is downward and negative, but is shown as a positive value
490 in this figure. As expected, the total mobilized side shear force increases approximately linearly
491 with increasing changes in temperature. The total mobilized side shear force should be equal and
492 opposite to the end bearing of the foundation to ensure external equilibrium. It is important to
493 note that the end bearing due to heating of the foundation should be less than or equal to the
494 maximum thermal axial stress for fully constrained conditions calculated using Equation (2). The

maximum thermal axial stress for each change in temperature is also shown in Figure 7(b), and except in the first two heating increments where the thermal axial stress profile does not monotonically increase with depth due to strain gage variability, the total mobilized side shear force is less than the maximum possible thermal axial stress.

Profiles of the thermal axial strain, displacement, and stress after each of heating and cooling cycles are shown in Figures 8(a), 8(b), and 8(c), respectively. During cooling from 39 to 30 °C, negative, expansive strains are still present in the foundation. The thermal axial strain near the head of the foundation decreases by a greater amount than deeper in the soil layer. The theoretical free-expansion thermal axial strain values calculated using Eq. (1) are shown in Figure 8(a) at a depth of 0 m, and they correspond well with the measured thermal axial strain values. The thermal axial displacements in the energy foundation do not change significantly except at the head of the foundation, and the thermal head displacements obtained from Figure 5(b) are relatively consistent with the thermal strain measurements. The thermal axial stress remained higher near the base of the foundation during the cooling process.

The maximum and minimum thermal head displacements during each of the heating cycles for the end-bearing foundation are shown in Figure 9(a). At the end of the first heating stage, the head of the foundation has an upward, prototype-scale displacement of -1.40 mm. During cooling back to a temperature of 30 °C, the foundation did not contract back to its original position as it was not cooled back to ambient temperature. During each subsequent heating stage, the foundation expanded slightly less than the previous cycle, although the difference between the expansion and contraction of the foundation during each cycle was similar (upward expansion of -1.26 mm after 4 cycles). The reason for the lower magnitude of axial expansion during each heating cycle could be due to either changes in the effective stress state around the

518 foundation arising from thermally-induced water flow away from the foundation, or the effects
519 of the differential settlement between the soil and foundation during centrifugation. During the
520 heating cycles, the maximum and minimum thermal axial stress in the end-bearing foundation,
521 shown in Figure 9(b), showed no significant change. This indicates that the changes in the soil
522 behavior during transient heating and cooling did not have a major impact on the thermo-
523 mechanical response of the energy foundation.

524 The results from the centrifuge physical modeling test presented in this study highlight some
525 of the advantages and limitations of centrifuge physical modeling of thermo-mechanical soil-
526 structure interaction in energy foundations. Advantages include the incorporation of dense
527 instrumentation arrays, control of soil layering and end-restraint boundary conditions, and the
528 ability to follow mechanical and thermal loading paths that may be difficult to perform in the
529 field. The centrifuge may also be useful for evaluating the role of soil behavior on the response
530 of energy foundations, especially in the case for challenging soil profiles such as unsaturated
531 soils or soft clays. It is often easier to assess the transient behavior of these soil profiles in a
532 centrifuge model than in a full-scale soil layer. One issue with centrifuge modeling of this type
533 of problem is that waiting for steady-state heat flow may be time consuming, especially when
534 studying the effects of heating and cooling. Although an understanding of the response of energy
535 foundations during transient heating and cooling is useful, reaching steady-state conditions will
536 ensure that all effects of thermo-mechanical soil behavior have been expressed and will lead to
537 the most accurate calibration of load-transfer analyses. Another issue is that application of
538 scaling relationships causes events related to heat transfer by conduction to occur faster in the
539 model than in the prototype, meaning that a greater volume of soil will be affected by
540 temperature changes in the model than in the prototype. Although the results from thermo-

mechanical tests may represent a worst-case scenario due to the greater zone of influence of the foundation, evaluation of time-dependent processes is complicated to consider. Nonetheless, finite element models can still be validated using the model-scale response of the energy foundations. Another issue is that the method of installing the energy foundations in the centrifuge can never replicate the process of installation and curing encountered in the field. An implication of this issue is that the soil-foundation interface cannot be replicated in a centrifuge model, even though the interface may have an important effect on the restraint of thermal movements of an energy foundation.

CONCLUSIONS

The behavior of a scale-model energy foundation tested in a geotechnical centrifuge during transient heating and cooling agrees well with observations from full-scale end-bearing energy foundations reported in the literature. Although limitations may be encountered in scaling of heat transfer processes and the use of transient heating and cooling for characterization, the results from this study confirm the relevance of centrifuge modeling of energy foundations to provide data for calibration and validation of soil-structure interaction models or to verify hypotheses about the relative impacts of end-restraint boundary conditions and side shear resistance. The results from staged heating tests on an end-bearing foundation indicate that the maximum thermal axial stress occurs near the base, likely due to an increase in side shear resistance with depth. The thermal axial strains were consistently less than the free-expansion thermal strain, and the thermal axial displacements calculated by integrating the thermal axial strains correspond well with the thermal head displacements measured independently with an LVDT. The mobilized side stresses calculated from the thermal axial stresses increased with height and were consistent with the shear strength of unsaturated silt. The instrumentation in the centrifuge

564 experiment was found to permit assessment of possible mechanisms leading to changes in soil
565 behavior during cyclic heating, an aspect which would have been difficult in a full-scale
566 foundation. During successive heating-cooling cycles, slight decreases in upward thermal head
567 displacement were observed due to changes in stiffness of the unsaturated soil due to thermally-
568 induced water flow away from the foundation and potential down-drag effects. Nonetheless, little
569 change in the maximum thermal axial stress was observed during the heating-cooling cycles
570 indicating that the foundation was relatively unaffected by the heating and cooling cycles.
571 Although the results in this study do not indicate that thermo-hydro-mechanical effects in the soil
572 layer lead to significant changes in foundation behavior, they are important to consider when
573 interpreting the thermal axial strain, displacement and stress response of energy foundations.

574 **ACKNOWLEDGMENTS**

575 The authors would like to thank undergraduate students Joseph Goode III and Michael Fend,
576 as well as centrifuge engineers Nathaniel Bailey and Kent Polkinghorne for their help with
577 centrifuge testing. Discussions with Kyle Murphy are greatly appreciated. Financial support from
578 NSF grant CMMI-0928159 is gratefully acknowledged. The contents of this paper reflect the
579 views of the authors and do not necessarily reflect the views of the sponsor.

APPENDIX I. REFERENCES

Amatya, B.L., Soga, K., Bourne-Webb, P.J., Amis, T., and Laloui, L. (2012). "Thermo-mechanical behaviour of energy piles." Géotechnique 62(6), 503–519.

Bouazza, A., Singh, R.M., Wang, B., Barry-Macaulay, D., Haberfield, C., Chapman, G., Baycan, S., and Carden, Y. (2011). "Harnessing on site renewable energy through pile foundations." Australian Geomechanics. 46(4), 79-90.

Bourne-Webb, P.J., Amatya, B., Soga, K., Amis, T., Davidson, C. and Payne, P. (2009). "Energy pile test at Lambeth College, London: Geotechnical and thermodynamic aspects of pile response to heat cycles." Géotechnique. 59(3), 237–248.

Brandl, H. (1998). "Energy piles and diaphragm walls for heat transfer from and into the ground." Proceedings of the 3rd International Geotechnical Seminar on Deep Foundations on Bored and Auger Piles, BAP III, Ghent, Belgium. October 19-21. Balkema, Rotterdam. 37–60.

Brandl, H. (2006). "Energy foundations and other thermo-active ground structures." Géotechnique. 56(2), 81-122.

Ennigkeit, A. and Katzenbach, R. (2001). "The double use of piles as foundation and heat exchanging elements." Proceedings of the 15th International Conference on Soil Mechanics and Geotechnical Engineering. Istanbul, Turkey. 893-896.

Goode, J.C., III. (2013). Centrifuge Modeling of the Thermo-Mechanical Response of Energy Foundations. MS Thesis. University of Colorado Boulder. 221 pg.

Hughes, P.J. (2008). Geothermal (Ground-Source) Heat Pumps: Market Status, Barriers to Adoption, and Actions to Overcome Barriers. Oak Ridge National Laboratory Report ONRL-2008/232.

603 Knellwolf, C., Peron, H., and Laloui, L. (2011). “Geotechnical analysis of heat exchanger piles.”
604 Journal of Geotechnical and Geoenvironmental Engineering. ASCE. 137(12), 890-902.
605 Ko, H.-Y. (1988). “Summary of the state-of-the-art in centrifuge model testing.” Centrifuges in
606 Soil Mechanics. Craig, James, Scofield, eds. Balkema, 11-28.
607 Krishnaiah, S. and Singh, D.N. (2004). “Centrifuge modelling of heat migration in soils.”
608 International Journal of Physical Modelling in Geotechnics. 4(3), 39-47.
609 Laloui, L. (2011). “In-situ testing of heat exchanger pile.” GeoFrontiers 2011. Dallas, TX. March
610 13-16th, 2011. ASCE. 10 pg.
611 Laloui, L., Moreni, M. and Vulliet, L. (2003). “Comportement d’un pieu bi-fonction, foundation
612 et échangeur de chaleur.” Canadian Geotechnical Journal. 40(2), 388-402.
613 Laloui, L., Nuth, M. and Vulliet, L. (2006). “Experimental and numerical investigations of the
614 behaviour of a heat exchanger pile.” International Journal of Numerical and Analytical
615 Methods in Geomechanics. 30(8), 763–781.
616 Laloui, N. and Nuth, M. (2006). “Numerical modeling of some features of heat exchanger pile.”
617 Foundation Analysis and Design: Innovative Methods (GSP 153). ASCE. Reston, VA.
618 pp. 189-195.
619 McCartney, J.S. and Rosenberg, J.E. (2011). “Impact of heat exchange on side shear in thermo-
620 active foundations.” GeoFrontiers 2011. Dallas, TX. March 13-16th, 2011. ASCE. 10 pg.
621 McCartney, J.S. and Murphy, K.D. (2012). “Strain distributions in full-scale energy
622 foundations.” DFI Journal. 6(2). 28-36.
623 Plaseied, N. (2011). Load-Transfer Analysis of Energy Foundations. M.S. Thesis. University of
624 Colorado Boulder. 90 pg.

625 Regueiro, R., Wang, W., Stewart, M.A., and McCartney, J.S. (2012). "Coupled thermo-poro-
626 mechanical finite element analysis of a heated single pile centrifuge experiment in
627 saturated silt." GeoCongress 2012. Oakland, CA. March 25-29th 2012. ASCE. 10 pg.
628 Rosenberg, J.E. (2010). Centrifuge Modeling of Soil Structure Interaction in Thermo-Active
629 Foundation. M.S. Thesis. University of Colorado Boulder. 125 pg.
630 Stewart, M. (2012). Centrifuge Modeling of Strain Distributions in Energy Foundations. MS
631 Thesis. University of Colorado Boulder. 110 pg.
632 Savvidou, C. (1988). "Centrifuge modelling of heat transfer in soil." Proceedings of Centrifuge
633 88, Corté, ed., Balkema, Rotterdam. 583-591.
634 Taylor R. (1995). Geotechnical Centrifuge Technology. Blackie, London. 296 p.
635 Vishay Precision Group. (2011). Personal communication with Jim Jones.
636 Uchaipichat, A. and Khalili, N. (2009). "Experimental investigation of thermo-hydro-mechanical
637 behaviour of an unsaturated silt." Géotechnique 59(4), 339–353.
638 Wang, B., Bouazza, A., Barry-Macaulay, D., Singh, M.R., Webster, M., Haberfield, C.,
639 Chapman, G., and Baycan, S. (2012). "Field and laboratory investigation of a heat
640 exchanger pile." GeoCongress 2012. Oakland, CA. March 28-30th, 2012. ASCE. 10 pg.
641

LIST OF TABLE AND FIGURE CAPTIONS

Table 1: Geotechnical properties of Bonny silt and soil placement conditions in the energy foundation test

Fig. 1. Schematics of the scale model energy foundation including locations of instrumentation

Fig. 2. Locations of instrumentation in the energy foundation tests

Fig. 3. Schematic of the temperature control system for centrifuge testing

Fig. 4. Measured temperatures for the end-bearing foundation: (a) Inlet and outlet fluid temperatures with the ambient centrifuge temperature; (b) Internal temperatures in the foundation; (c) Comparison between the average temperatures of the energy foundations and surrounding soil

Fig. 5. Primary test variables: (a) Axial stress and average change in temperature of the energy foundation; (b) Thermo-mechanical displacements in model and prototype scale along with the thermal head displacements in prototype scale; (c) Thermal axial strains at different prototype depths; (d) Change in volumetric water content of the unsaturated silt at different model-scale depths a model-scale distance of 50 mm from the foundation

Fig. 6. Profiles of thermo-mechanical response during initial heating stages (prototype scale): (a) Thermal axial strain; (b) Thermal axial displacement; (c) Thermal axial stress

Fig. 7. Mobilized side shear resistance during initial heating stages (prototype scale): (a) Mobilized side shear stress profiles; (b) Comparison of total mobilized side shear stress and maximum thermal axial stress

Fig. 8. Profiles of thermo-mechanical response after successive heating-cooling cycles (prototype scale): (a) Thermal axial strain; (b) Thermal axial displacement; (c) Thermal axial stress

665 **Fig. 9**. Synthesis of foundation and soil responses after successive heating cycles (prototype
666 scale): (a) Change in thermal head displacement; (b) Change in thermal axial stress
667

668 **Table 1:** Geotechnical properties of Bonny silt and soil placement conditions in the energy
669 foundation test

Parameter	Value
D_{10}	< 0.0013 mm
D_{30}	0.022 mm
D_{50}	0.039 mm
% Passing No. 200 Sieve	83.9 %
% Clay Size	14.0 %
% Silt Size	69.9 %
% Sand Size	16.1 %
G_s	2.6
Liquid Limit, LL	25
Plastic Limit, PL	21
Plasticity Index, PI	4
Activity, A	0.29
Effective friction angle, ϕ	32.4°
Compression index, C_c	0.015
Recompression index, C_r	0.0017
Std. Proctor Max. Dry Unit Weight	16.9 kN/m^3
Std. Proctor Max. Opt. Water Content	13.6%
Drying-path soil water retention curve*	$a_{VG} = 0.035$ kPa^{-1}, $N_{VG} = 1.77$, $\theta_r = 4\%$
Initial void ratio, e_0	0.63
Initial water content, w_0	14.2%
Initial degree of saturation, S_0	0.59
Saturated hydraulic conductivity, k_s	7.6×10^{-8} m/s
Thermal conductivity for e_0 and S_0, λ	1.147 W/mK

670 *Defined using the van Genuchten (1980) model

671

Figure 1
Click here to download high resolution image

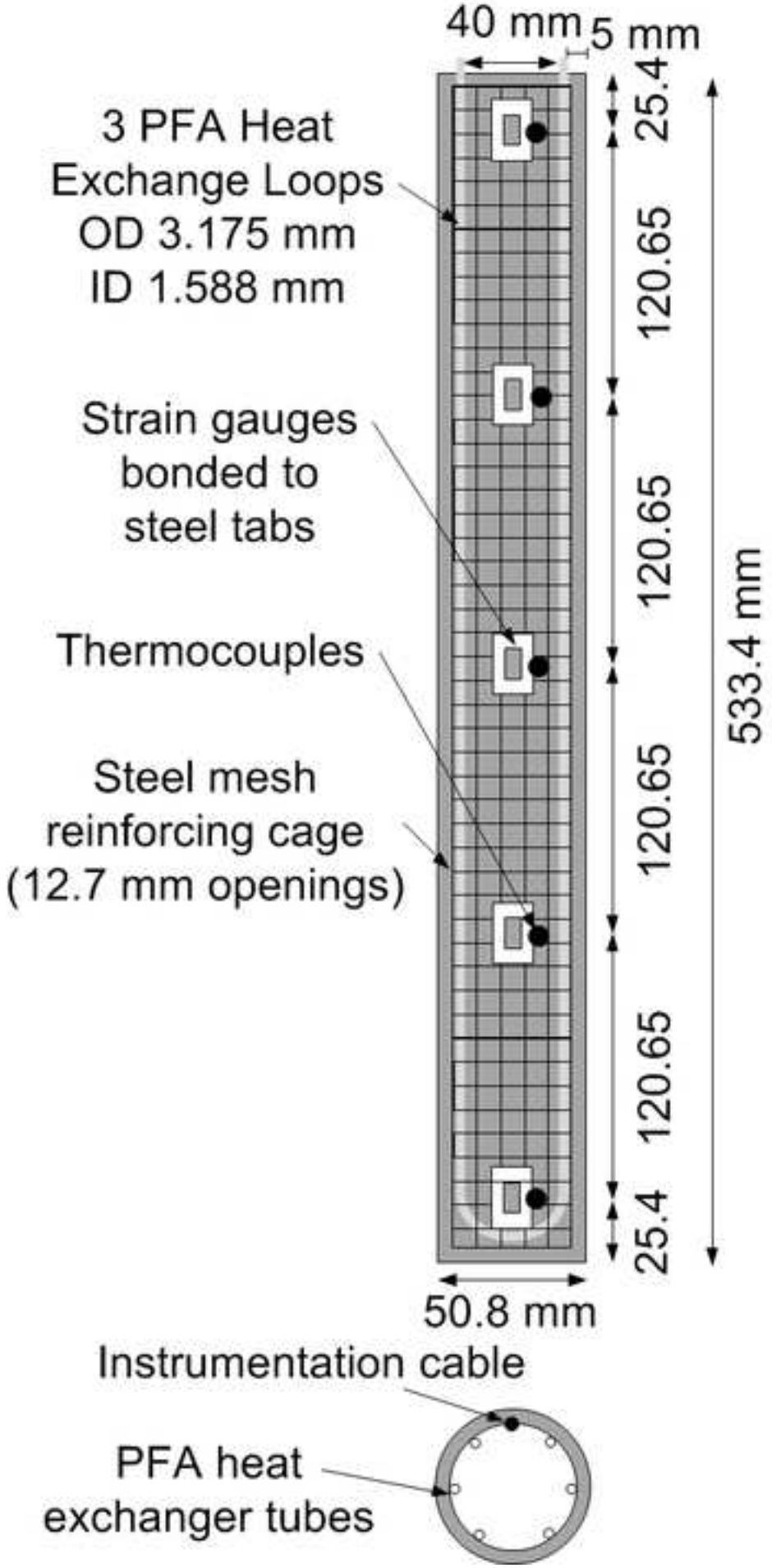

Figure 2
Click here to download high resolution image

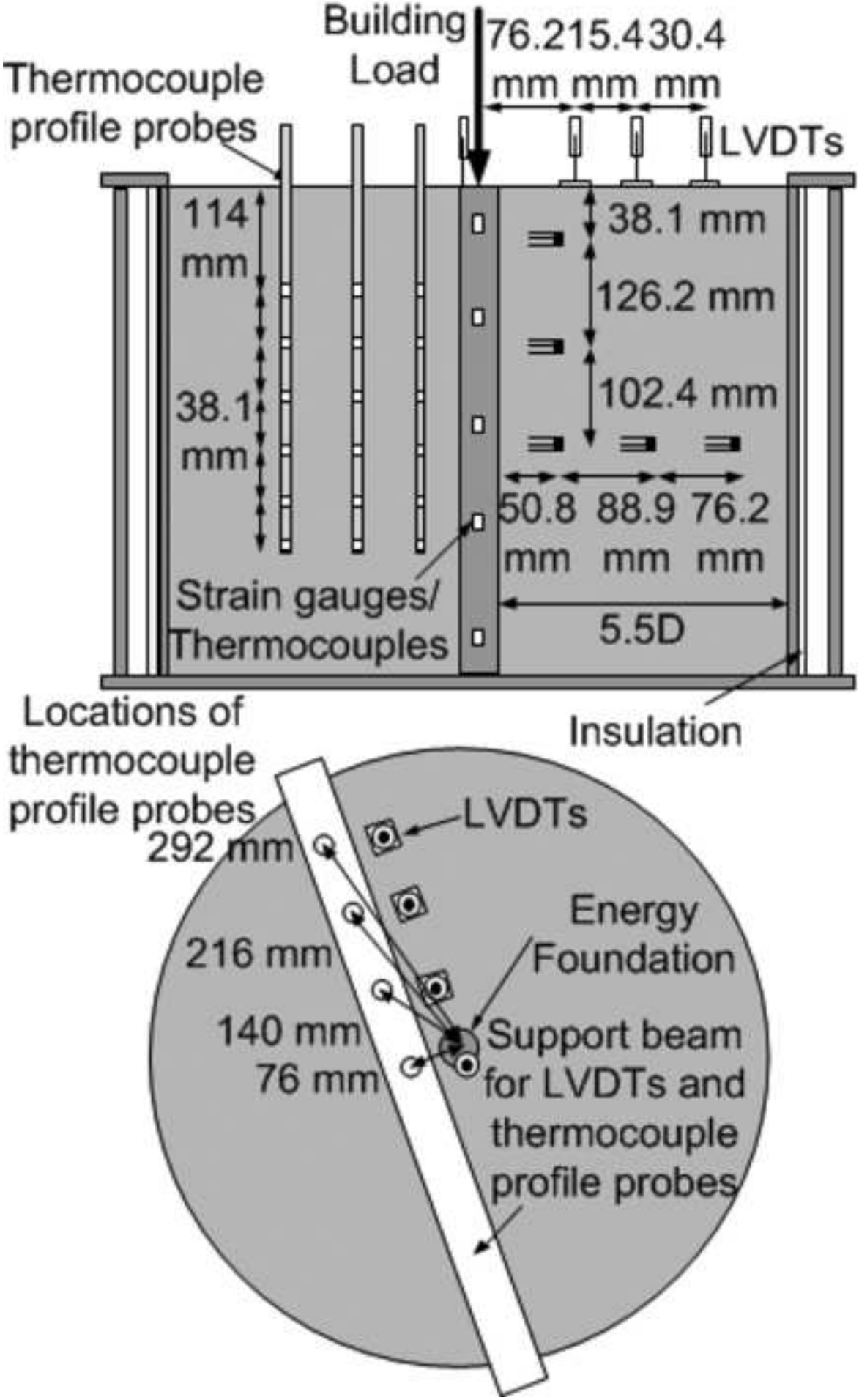

Figure 3
Click here to download high resolution image

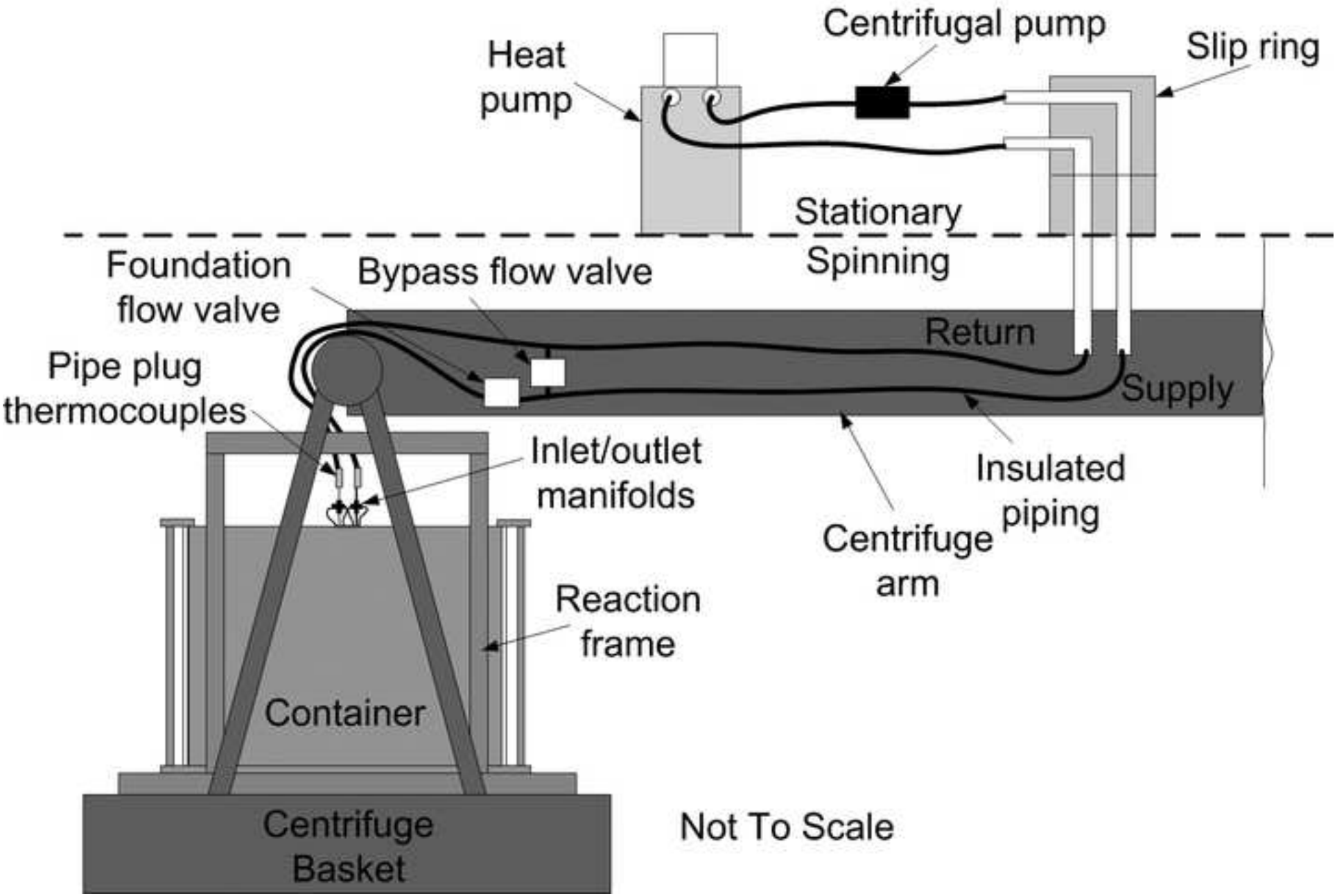

Figure 4
Click here to download high resolution image

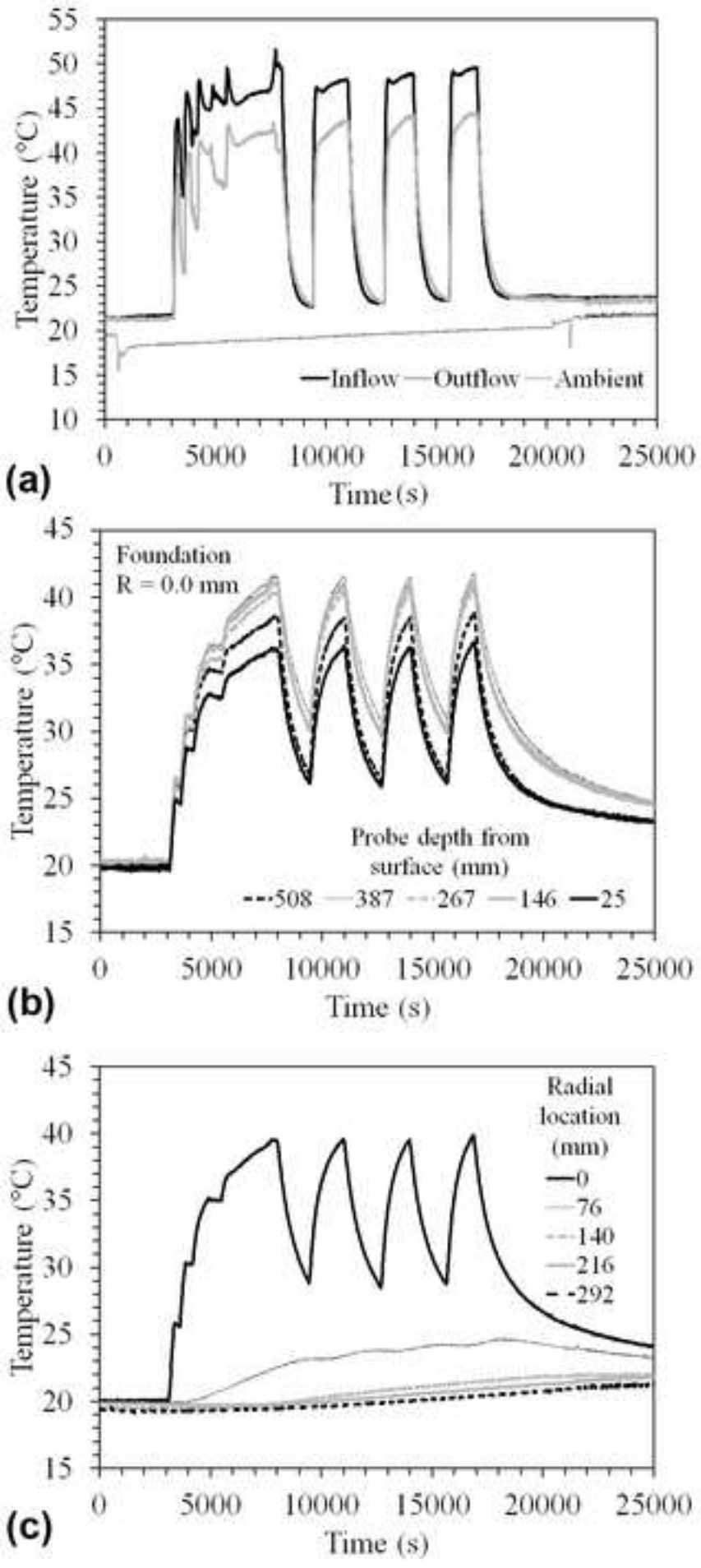

Figure 5
Click here to download high resolution image

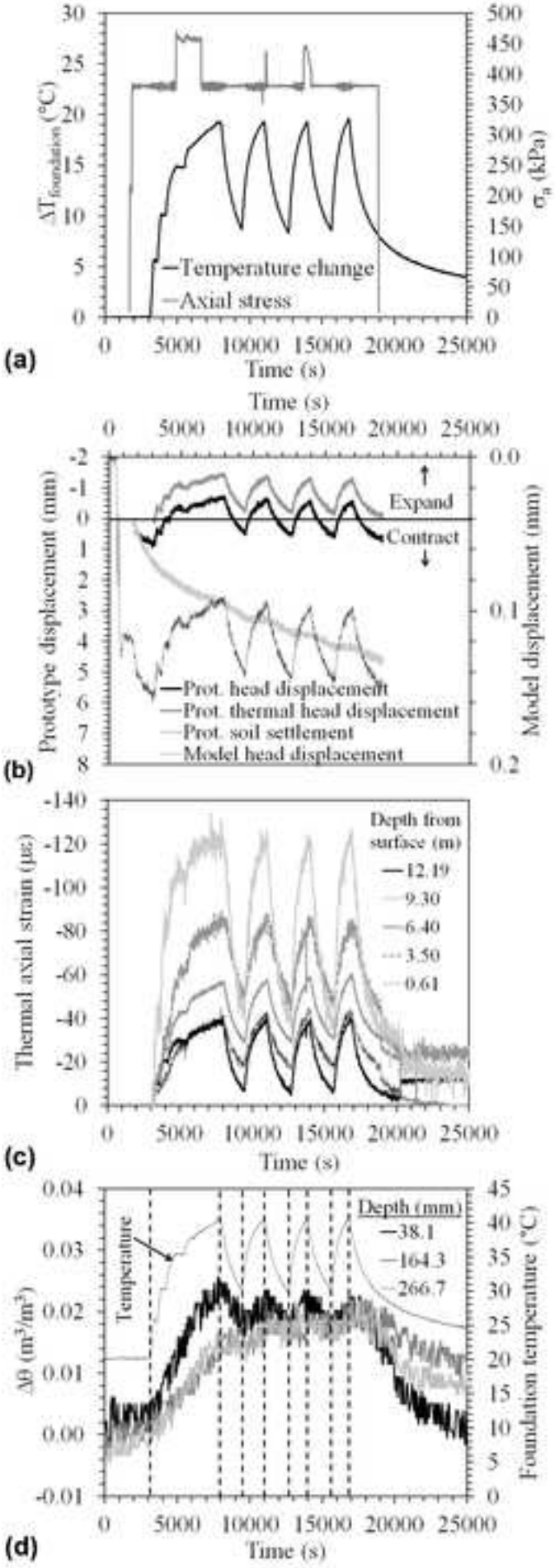

Figure 6
Click here to download high resolution image

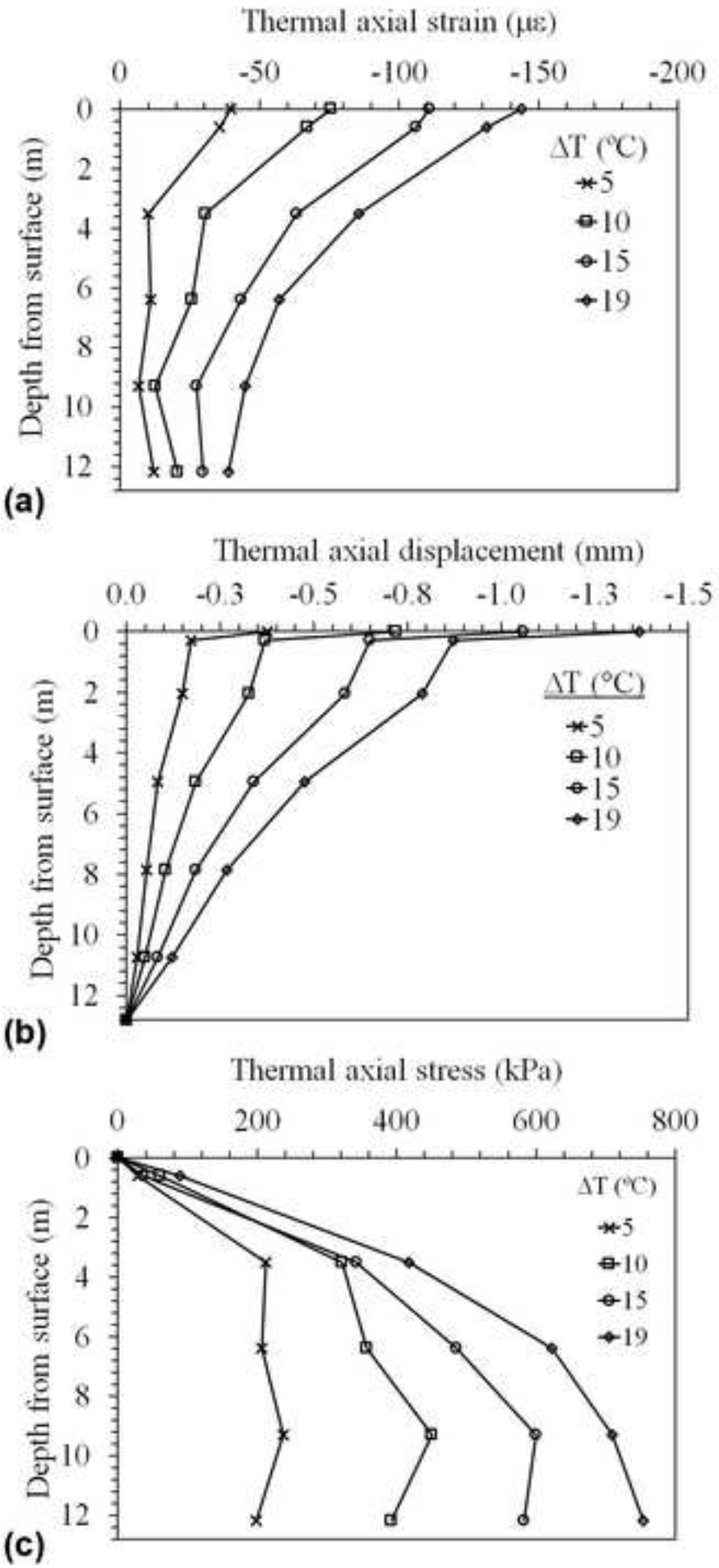

Figure 7
Click here to download high resolution image

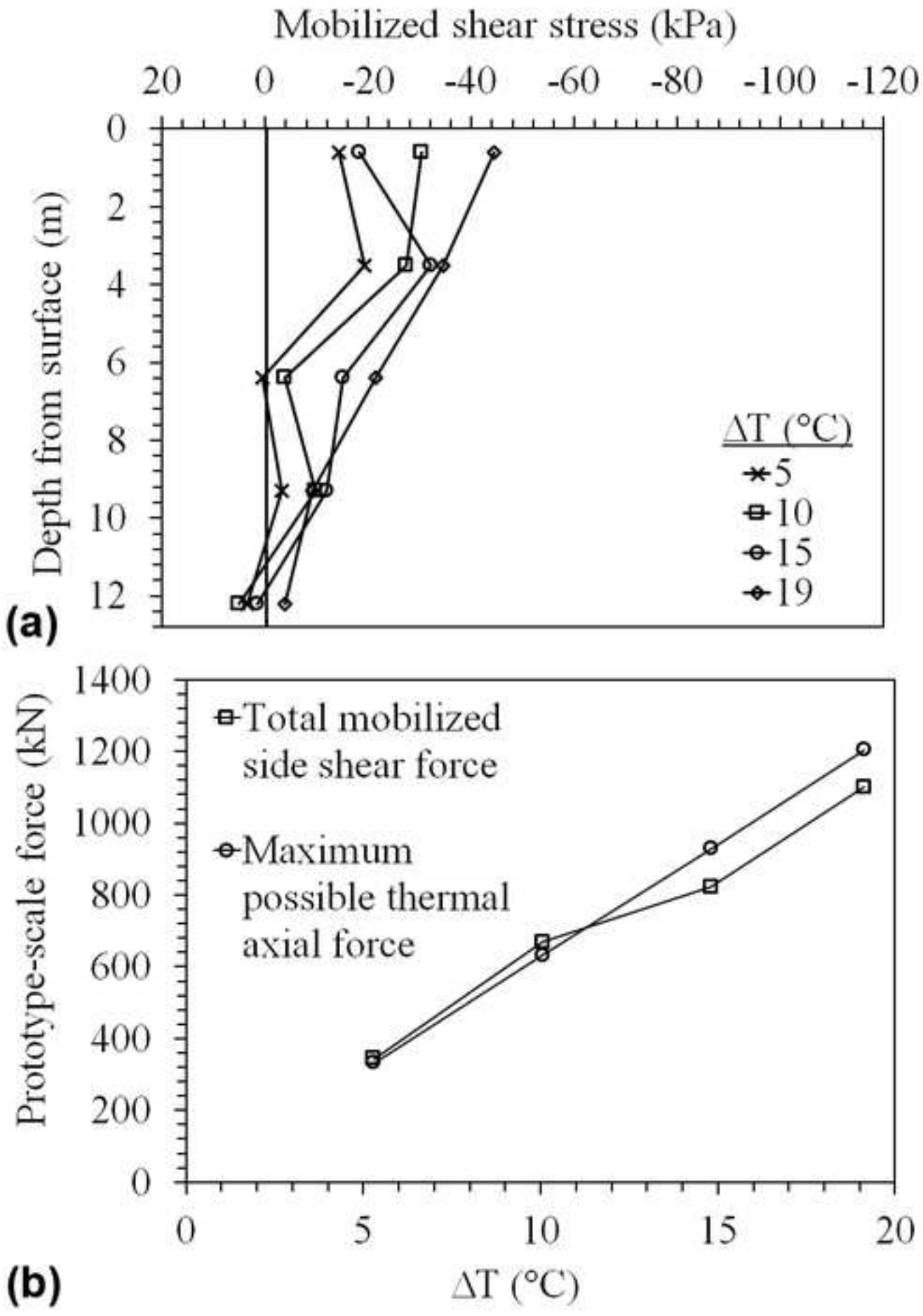

Figure 8
Click here to download high resolution image

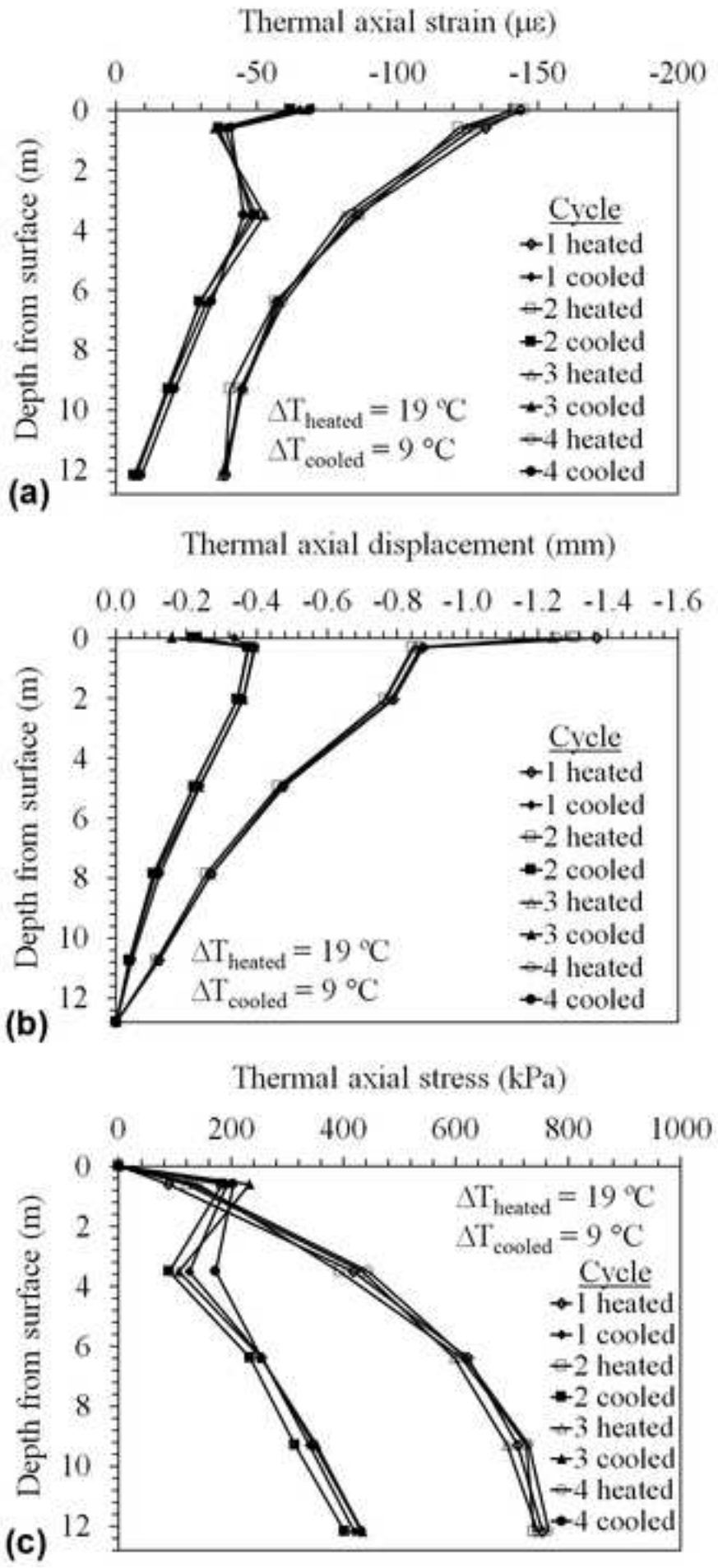

Figure 9
Click here to download high resolution image